Combination of Topology Optimization and Lie Derivative-based shape optimization for electro-mechanical design

Erin Kuci[a,b], François Henrotte[b,c], Pierre Duysinx[a], Christophe Geuzaine[b]

[a] *University of Liège, Department of Aerospace and Mechanical Engineering, Belgium*
[b] *University of Liège, Department of Electrical Engineering and Computer Science, Belgium*
[c] *Université catholique de Louvain, EPL-iMMC-MEMA, Belgium*

Abstract

This paper presents a framework for the simultaneous application of shape and topology optimization in electro-mechanical design problems. Whereas the design variables of a shape optimization are the geometrical parameters of the CAD description, the design variables upon which density-based topology optimization acts represent the presence or absence of material at each point of the region where it is applied. These topology optimization design variables, which are called *densities*, are by essence substantial quantities. This means that they are attached to matter while, on the other hand, shape optimization implies ongoing changes of the model geometry. An appropriate combination of the two representations is therefore necessary to ensure a consistent design space as the joint shape-topology optimization process unfolds. The optimization problems dealt with in this paper are furthermore constrained to verify the governing partial differential equations (PDEs) of a physical model, possibly nonlinear and discretized by means of, e.g., the finite element method (FEM). Theoretical formulas, based on the Lie derivative, to express the sensitivity of the performance functions of the optimization problem are derived and validated to be used in gradient-based algorithms. The method is applied to the torque ripple minimization in an interior permanent magnet synchronous machine (PMSM).

Keywords: Lie derivative, Shape Optimization, Topology Optimization, Sensitivity Analysis, Simultaneous Shape and Topology, PMSM

Contents

Email address: Erin.Kuci@ulg.ac.be (Erin Kuci)

1. Introduction

Industrial design issues in structural engineering have been handled over the years by applying either shape optimization [1, 2] or topology optimization [3, 4, 5]. Shape optimization finds out the optimal layout within the design space determined by the geometrical parameters of the CAD description of the model. Density-based topology optimization, on the other hand, optimally removes material in a structure, holding its strength between prescribed limits. The latter is characterized by its ability to find optimal layouts with sometimes unusual contours and unexpected holes, but in general significantly lighter (in weight). There is therefore a desire to combine the two optimization methods in order to reach better performances.

Several strategies intended to handle the complex interactions between shape and topology optimizations have been developed so far. Among existing methods, adaptive topology optimization has been performed to form an explicit interface between the solid and void regions which arise throughout a structural density-based topology optimization, see for instance [6]. More recently, a similar paradigm has been followed by [7, 8] to adapt to topology optimization the deformable simplicial complex (DSC) method [9] which simulates fluids accurately. Here, both the design and the analysis models rely on the same spatial discretization. The DSC deformation is therefore used to adapt the mesh after the movement of the interface, such that it is well formed, and involves a series of mesh operations, e.g. Laplacian smoothing, edge flip, vertex insertion and vertex removal, which are quite artificial.

Level set methods, which were originally proposed for numerically tracking free boundaries are among alternative approaches to density-based topology optimization [10]. In this context, the geometry is represented as the zero level set of functions and are propagated through the solution of Hamilton-Jacobi type equations. This approach, which allows to easily handle large shape modifications without requiring a CAD representation, has been first applied to structural optimization, see [11, 12], but also in electromagnetic design of electrical rotating machines and inverse problems, see for instance [13, 14]. The method can advantageously be carried out in a fixed mesh. Furthermore, the topological complexity of classical CAD based shape optimization is reduced since geometric entities, such as holes, can be merged or removed without degenerating the model, but unfortunately cannot be created, except if the method is combined with a topological derivative (see for instance [15, 16, 17, 18, 19] or [20] for more theoretical aspects). However, the use of a level set representation of the geometry makes it difficult to take into account geometries with sharp angles (see for instance [21] or [22]). It limits hence the range of systems that can be optimized.

Topology and shape optimizations have also been coupled in the context of packaging. For instance, the position [23] and shape [24] of the packaged items are determined by a shape optimization process while, at the same time, the protective material usage is minimized by means of a density-based topology optimization, [25, 26], so as to, e.g., minimize the overall volume of the package. An alternative approach with a fixed mesh is also possible. A level set representation of the component boundaries is used, instead of a CAD representation, and the model is solved with an extended finite element method (XFEM) [24].

In all cases, a gradient-based algorithm is preferred to solve the combined shape and topology optimization problems as it leads to fewer simulations of the underlying PDE model. A substantial gain in computation time is furthermore obtained when sensitivities, i.e., the derivatives of the performance functions with respect to the design variables, are obtained analytically (prior

to discretization) by differentiation under the integral sign of the PDEs variational form instead of evaluating a finite difference, which requires one additional solution of the physical problem for each design variable. In the continuous context, prior to discretization, the variation of the residual related to the physics of the problem with respect to a design variable that controls the material density distribution can be expressed explicitly, in general, by means of the total derivative, as suggested by e.g. [27]. However, the variation of the residual with respect to a design variable that brings modifications in the boundaries of the system is more delicate to express, and requires terms to account for the implicit dependency of the residual in the continuous flow of geometrical modification.

Analytical shape sensitivities have been obtained in the past through the velocity method, as introduced in [28]. This approach uses the variation of the shape design variable as the parameter describing a smooth geometrical transformation of the domain, with no tearing nor overlapping, that brings the boundaries of the domain from their unperturbed position to their perturbed position. The variation of the parameter determines therefore a flow characterized by a velocity field. The velocity method has been applied successively to elasticity problems where the solution of the physical problem is a scalar field, see for instance [24]. Following this approach, analytical formulas have also been proposed in other disciplines such as electromagnetics, based on classical vector analysis, as in [29, 30]. However, these works have been exclusively devoted to problems expressed in terms of a scalar unknown field, leaving aside the problem of handling the complex behavior of a vector field under the transformation that brings a modification of the system boundaries. To handle the shape derivative of vector fields, one can refer to a more general theoretical framework based on the exterior calculus, well established so far in mathematical modeling and analysis of PDEs, e.g. [31, 32], borrowed from differential geometry, and in particular the concept of Lie derivative. These material derivatives have been used more recently by [33] in order to overcome the limitations and the tedious calculations of the vector analysis approach, classically used for the scalar field. This approach has been applied to the sensitivity calculation of a linear acoustic and electromagnetic boundary integral problems [34]. We have shown in [35] that using the Lie derivative, sensitivities for more complex problems (non linear electromagnetic and elastic) can be efficiently computed in both 2D and 3D thanks to a velocity field based on the parametrization of the geometric model of the domain. On a practical level, this approach is very efficient since it limits the support of the volume integrals involved in the sensitivity formulas to a one layer thick layer of finite elements on both sides of the surfaces involved in the shape variation. The resulting formulas, expressed in classical vector analysis form, constitute an easy-to-apply formula sheet for deriving the sensitivity of any vector field.

In this paper, we propose to tackle the combined shape and topology optimization problem by solving an adjoint formulation by a sequential gradient-based convex programming approach, [36, 37], called Method of Moving Asymptotes (MMA) in which local approximations of the performance functions are built as convex and separable approximations (called subproblems). In our combined shape and topology optimization approach, we compute the sensitivities analytically based on the construction of a velocity field and on the Lie derivative as proposed in [35]. The paper is organized as follows. The general optimization problem is posed in Section 2 and the parameterization of the design space is discussed in Section 3. Section 4 deals with the theoretical definition of the sensitivities associated with both the density and the shape variables and provide analytic formulas to evaluate them practically. In Sections 5, the joint shape-topology optimization is applied to the torque ripple minimization in an interior permanent magnet machine.

2. Optimization in mixed shape and topology design spaces

A 3-phase permanent magnet synchronous motor (PMSM) is an electro-mechanical energy converter which transforms electric energy into mechanical energy. It consists of a fixed part, called the stator, with windings fed by a sinusoidal current, and a rotating part, called the rotor, with permanent magnets, and separated by an airgap, see Fig. 1. This machine produces torque, which can exhibit very high level of ripples. We model the geometry of the PMSM as a bounded domain Ω (rotor and stator), by means of a CAD model. Taking advantage of the symmetries of the physical field, only $1/8^{th}$ of the overall geometry is considered. Moreover, the spatial discretization of the rotor and the stator remain unchanged as the rotor changes positions, and are connected by a single layer of elements in the moving band, which is remeshed for each rotor position [38].

The bounded domain Ω undergoes both shape and topology modifications. The shape modifications are controlled by a set of geometrical design variables, noted τ, of the CAD model description. Topology optimization acts, on the other hand, on design variables which we call densities, noted ρ. They represent the presence or not of a specific material at each point of model region where it is applied. Topology optimization offers a great flexibility in the design since it allows for an improvement of the material usage while shape optimization, on the other hand, allows for a fine tuning of the geometrical parameters.

A family of mappings,

$$p_{\delta\tau} : \Omega(\tau) \subset E^3 \mapsto \Omega(\tau + \delta\tau) \subset E^3, \tag{1}$$

describes the geometrical modification of Ω in the Euclidean space E^3, with no tearing nor overlapping, and it is parameterized by the set of geometrical design variables τ, see [28]. A variation $\delta\tau$ of the shape variable brings the interfaces and the points of Ω from their current position to their modified position. A flow with a velocity field noted $\mathbf{v}$ is determined on E^3 by varying $\delta\tau$ in the family of mappings (1) in a neighborhood of zero, see [35]. The parameter $\delta\tau$ plays therefore the role of a pseudo time variable. The value of the density, on the other hand, at a given point in the region Ω_ρ (the whole rotor) of the model is obtained by evaluating that field at the coordinates of that point. However, the variation $\delta\rho$ of the density field ρ does not involve any movement of the physical interfaces of Ω.

The system is modeled in terms of a magnetostatic formulation, written at the continuous level by its weak formulation. It reads: find $\boldsymbol{A}^\star$ the magnetic vector potential verifying appropriate boundary conditions such that the residual

$$r(\tau, \rho, \boldsymbol{A}^\star, \bar{\boldsymbol{A}}) = \int_{\Omega(\tau)} \nu(\rho, \mathbf{curl}\, \boldsymbol{A}^\star)\, \mathbf{curl}\, \boldsymbol{A}^\star \cdot \mathbf{curl}\, \bar{\boldsymbol{A}} - \boldsymbol{J} \cdot \bar{\boldsymbol{A}} - \boldsymbol{M} \cdot \mathbf{curl}\, \bar{\boldsymbol{A}}\ \mathrm{d}\Omega = 0, \tag{2}$$

for appropriate test function $\bar{\boldsymbol{A}}$, [39].

In (2), $\boldsymbol{B}^\star = \mathbf{curl}\, \boldsymbol{A}^\star$ is the magnetic flux density, $\boldsymbol{H}(\boldsymbol{B}^\star) = \nu(\rho, \mathbf{curl}\, \boldsymbol{A}^\star)\, \mathbf{curl}\, \boldsymbol{A}^\star$ is the magnetic field, with ν the reluctivity depending on $\boldsymbol{B}^\star$ (nonlinear material). It is written by means of the SIMP law, in the region Ω_ρ where topology optimization is applied,

$$\nu(\rho, \boldsymbol{B}^\star) = \nu_0 + \rho^p(\nu^\dagger(\boldsymbol{B}^\star) - \nu_0), \quad \text{in } \Omega_\rho, \tag{3}$$

with $\nu^\dagger$ the reluctivity of steel and ν_0 the reluctivity of air.

The design problem aims at determining simultaneously the geometrical design variables, τ, and the densities, ρ, that minimize a cost function $f_0(\tau, \rho, \boldsymbol{A})$, subjected to m inequalities $f_j(\tau, \rho, \boldsymbol{A}) \leq 0$, $j = 1, \ldots, m$, ensuring the manufacturability or the feasibility of the design. The design space is also limited by side constraints either for the shape design variables, $\tau^{min} \leq$

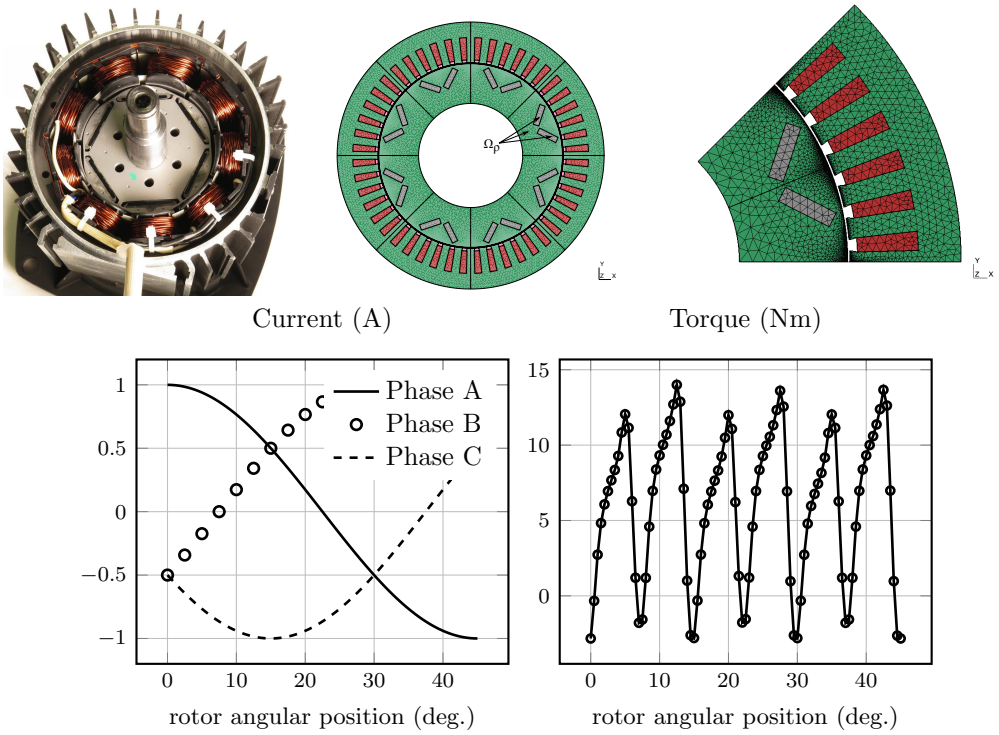

Figure 1: A slice of a 3-phase interior permanent magnet synchronous machine (PMSM), top, is considered. The PMSM is fed by a 3-phase sinusoidal current, bottom left, and produces torque, bottom right, which exhibits very high level of ripples. (Credit: Linz Center of Mechatronics (LCM), motor was produced by Hanning Elektro-Werke GmbH & Co KG)

$\tau \leq \tau^{max}$, or the density design variables, $\rho^{min} \leq \rho \leq \rho^{max}$. The shape design variables are independent from the density design variables, but they are both involved in the performance functions. Hence, the optimization problem reads

$$\begin{aligned} \min_{\tau,\rho} \quad & f_0(\tau, \rho, \boldsymbol{A}^\star) \\ s.t. \quad & f_j(\tau, \rho, \boldsymbol{A}^\star) \leq 0,\ j = 1, \ldots, m \\ & \tau^{min} \leq \tau \leq \tau^{max} \\ & \rho^{min} \leq \rho \leq \rho^{max} \\ & r(\tau, \rho, \boldsymbol{A}^\star, \bar{\boldsymbol{A}}) = 0,\ \forall \bar{\boldsymbol{A}}. \end{aligned} \tag{4}$$

In this article, a sequential convex programming algorithm, e.g. MMA [40], is used, coupled with a finite element analysis code [41, 42] and makes use of the sensitivity of the problem (4) (the derivatives of the performance functions with respect to the shape design variables, and also with respect to the density design variables), in order to reduce the number of function evaluations and hence, limit the required number of resolutions of the finite element physical problem (2).

3. Shape and topology design spaces

State-of-the-art methods of density-based topology optimization represent the material densities by a field defined on a fixed grid, identical to the FEM grid, [43], while CAD-based shape optimization methods completely remesh the structure so as to preserve the quality of the FEM solution throughout the geometrical changes of the CAD model, see for instance [44].

In our approach, the densities are represented by a field defined on a fixed domain, noted Ω_ρ, not involved in the geometrical changes induced by the shape optimization, but covering in space all configurations allowed by it. The value of density at a point in the model is then simply the value of that field at the coordinates of the point. The modified CAD obtained by the variations of the shape design variables, are then discretized spatially by conformal meshes in order to carry out FEM analysis based on the material properties interpolated from the density field.

The shape design variables, τ, govern the CAD model description of the structure and their variation implies ongoing geometrical changes of the model, see Fig. 2. Each point $\boldsymbol{P}_\tau$, resp. $\boldsymbol{Q}_\tau$, is brought to a point $\boldsymbol{P}_{\tau+\delta\tau}$, resp. $\boldsymbol{Q}_{\tau+\delta\tau}$, as the shape design variables are perturbed by $\delta\tau$ and generates hence a velocity field, noted $\mathbf{v}$. The densities, denoted ρ, on the other hand, are represented by a discrete field defined on the fixed grid covering all configurations allowed by the variation of the geometrical design variable. The value of the density at a given point in the model, e.g. $\boldsymbol{P}_\tau$ or $\boldsymbol{Q}_\tau$, is then obtained by evaluating that field at the coordinates, x_1, x_2, x_3, of that point.

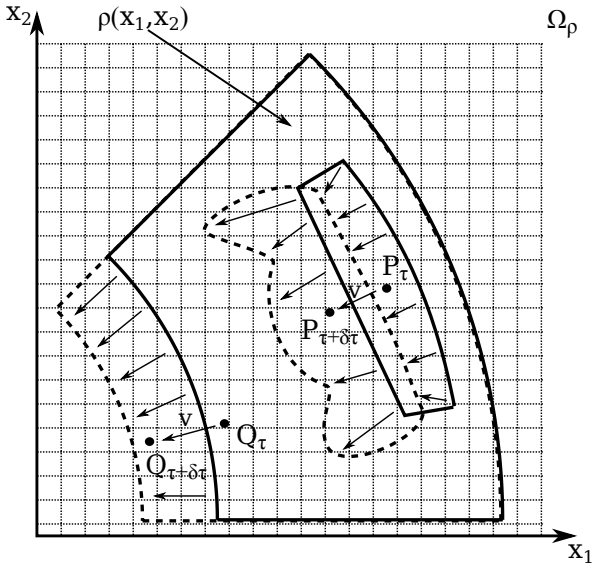

Figure 2: A 2D CAD model of a representative interior permanent magnet synchronous machine (PMSM) rotor is considered. The shape modifications are represented by means of a velocity field, noted $\mathbf{v}$.

4. Adjoint-based sensitivity analysis

We shall, for the sake of simplicity, consider one particular performance function $f(\tau, \rho, \boldsymbol{A})$, written explicitly in the form of an integral [1] evaluated at the solution $\boldsymbol{A}^\star$ of (2)

$$f(\tau, \rho, \boldsymbol{A}^\star) = \int_{\Omega(\tau)} F(\tau, \rho, \boldsymbol{A}^\star)\ \mathrm{d}\Omega, \tag{5}$$

where the function F depends explicitly on $\boldsymbol{A}^\star$, itself depending implicitly on the shape and density variables. The treatment of any other performance function will be similar.

4.1. Sensitivity with respect to density

The derivative of f with respect to ρ,

$$\frac{\mathrm{d}f}{\mathrm{d}\rho}(\tau, \rho, \boldsymbol{A}^\star) = \int_{\Omega(\tau)} \Big(D_\rho F(\tau, \rho, \boldsymbol{A}^\star) + \big\{ \mathrm{D}_{\boldsymbol{A}} F(\tau, \rho, \boldsymbol{A}^\star) \big\} \big(\frac{\mathrm{d}\boldsymbol{A}^\star}{\mathrm{d}\rho} \big) \Big)\ \mathrm{d}\Omega, \tag{6}$$

involves two terms. The first term is the partial derivative of the functional,

$$D_\rho F(\tau, \rho, \boldsymbol{A}^\star) = \frac{\mathrm{d}F}{\mathrm{d}\rho}(\tau, \rho, \boldsymbol{A}^\star)\Big|_{\frac{\mathrm{d}\boldsymbol{A}}{\mathrm{d}\rho}=0} \tag{7}$$

defined as the derivative holding the field argument $\boldsymbol{A}$ constant, while the second term involves the Fréchet derivative of the functional $F(\tau, \rho, \boldsymbol{A})$ with respect to its field argument $\boldsymbol{A}$, defined by

$$\lim_{|\delta\boldsymbol{A}|\to 0} \frac{1}{|\delta\boldsymbol{A}|} \Big| F(\tau, \rho, \boldsymbol{A} + \delta\boldsymbol{A}) - F(\tau, \rho, \boldsymbol{A}) - \big\{ \mathrm{D}_{\boldsymbol{A}} F(\tau, \rho, \boldsymbol{A}) \big\} \big(\delta\boldsymbol{A} \big) \Big| = 0, \tag{8}$$

where the limit is taken over all sequences of non-zero $\delta\boldsymbol{A}$ that converge to zero. The Fréchet derivative is a linear operator applied to the argument in between parenthesis outside the curly braces, $\mathrm{d}\boldsymbol{A}/\mathrm{d}\rho$, and evaluated in arguments between parenthesis inside the curly braces.

An augmented Lagrangian function is defined,

$$f_a(\tau, \rho, \boldsymbol{A}, \boldsymbol{\lambda}) = f(\tau, \rho, \boldsymbol{A}) - r(\tau, \rho, \boldsymbol{A}, \boldsymbol{\lambda}) \tag{9}$$

with $\boldsymbol{\lambda}$ a Lagrange multiplier. As (2) implies that the residual $r(\tau, \rho, \boldsymbol{A}^\star, \boldsymbol{\lambda})$ is zero at equilibrium, one has

$$f_a(\tau, \rho, \boldsymbol{A}^\star, \boldsymbol{\lambda}) = f(\tau, \rho, \boldsymbol{A}^\star), \tag{10}$$

and the sensitivity is expressed in terms of f_a by

$$\frac{\mathrm{d}f}{\mathrm{d}\rho}(\tau, \rho, \boldsymbol{A}^\star) = \frac{\mathrm{d}f_a}{\mathrm{d}\rho}(\tau, \rho, \boldsymbol{A}^\star, \boldsymbol{\lambda}). \tag{11}$$

The differentiation of (9) with respect to ρ yields

$$\begin{aligned} \frac{\mathrm{d}f_a}{\mathrm{d}\rho} = \int_{\Omega(\tau)} & \Big(D_\rho F(\tau, \rho, \boldsymbol{A}^\star) + \big\{ \mathrm{D}_{\boldsymbol{A}} F(\tau, \rho, \boldsymbol{A}^\star) \big\} \big(\frac{\mathrm{d}\boldsymbol{A}^\star}{\mathrm{d}\rho} \big) \\ & - \nu^\partial\, \mathbf{curl}\, \frac{\mathrm{d}\boldsymbol{A}^\star}{\mathrm{d}\rho} \cdot \mathbf{curl}\, \boldsymbol{\lambda} - (D_\rho \nu)\, \mathbf{curl}\, \boldsymbol{A}^\star \cdot \mathbf{curl}\, \boldsymbol{\lambda} + D_\rho \boldsymbol{J} \cdot \boldsymbol{\lambda} + D_\rho \boldsymbol{M} \cdot \mathbf{curl}\, \boldsymbol{\lambda} \Big)\, \mathrm{d}\Omega = 0, \end{aligned} \tag{12}$$

[1] If the performance function is a pointwise value, the expression of $F(\tau, \rho, \boldsymbol{A}^\star)$ will then involve a Dirac function.

where we have already omitted the null term, and where

$$\nu^{\partial}(\boldsymbol{B}) = \nu + \frac{\partial \nu}{\partial \boldsymbol{B}} \boldsymbol{B}$$

is the tangent reluctivity tensor of the material law.

Let now $\boldsymbol{\lambda}^\star$ be the solution of the following adjoint problem, proper to the performance function f,

$$\int_{\Omega(\tau)} \Big(\big\{ \mathrm{D}_{\boldsymbol{A}} F(\tau, \rho, \boldsymbol{A}^\star) \big\} \big(\frac{\mathrm{d}\boldsymbol{A}^\star}{\mathrm{d}\rho} \big) - \nu^{\partial} \, \mathbf{curl}\, \boldsymbol{\lambda} \cdot \mathbf{curl}\, \frac{\mathrm{d}\boldsymbol{A}^\star}{\mathrm{d}\rho} \Big) \, \mathrm{d}\Omega = 0, \tag{13}$$

which holds for all $\mathrm{d}\boldsymbol{A}^\star/\mathrm{d}\rho$. The system matrix of the adjoint problem (13) is the tangent stiffness matrix of the problem (2), i.e. the Jacobian matrix after finite element discretization and convergence of the iterative nonlinear process. It can be reused since the same discretization is used for solving (13) and (2).

Using (13) in (12), the sensitivity is given by

$$\begin{aligned} \frac{\mathrm{d}f_a}{\mathrm{d}\rho}(\tau, \rho, \boldsymbol{A}^\star, \boldsymbol{\lambda}^\star) = \int_{\Omega(\tau)} \Big(& D_\rho F(\tau, \rho, \boldsymbol{A}^\star) - D_\rho \nu \, \mathbf{curl}\, \boldsymbol{A}^\star \cdot \mathbf{curl}\, \boldsymbol{\lambda}^\star \\ & + D_\rho \boldsymbol{J} \cdot \boldsymbol{\lambda}^\star + D_\rho \boldsymbol{M} \cdot \mathbf{curl}\, \boldsymbol{\lambda}^\star \Big) \, \mathrm{d}\Omega \end{aligned} \tag{14}$$

in terms of the solutions of the nonlinear problem (2) and of the adjoint problem (13), where the partial derivative of reluctivity ν with respect to ρ is obtained analytically, e.g. for the SIMP law,

$$D_\rho \nu = p \; \rho^{(p-1)} (\nu^\dagger(\boldsymbol{B}) - \nu_0). \tag{15}$$

In our application, we consider that both $\boldsymbol{J}$ and $\boldsymbol{M}$ do not depend explicitly on ρ. Their partial derivatives $D_\rho \boldsymbol{J}$ and $D_\rho \boldsymbol{M}$ are hence both zero.

4.2. Sensitivity with respect to shape variation

Theoretical formulas to express the derivative of f with respect to a shape design variable τ have been demonstrated in detail using the Lie derivative in [35], in the context of the family of mappings (1), as introduced in [28].

Using the family of mappings (1), the Lie derivative of an arbitrary field ω (scalar field, vector field, or tensor field) in $\Omega(\tau)$ is defined as

$$L_{\mathbf{v}} \omega = \lim_{\delta\tau \to 0} \frac{p_{\delta\tau}^{-1} \omega - \omega}{\delta\tau}, \tag{16}$$

where the index $\mathbf{v}$ in the notation $L_{\mathbf{v}}\omega$ makes reference to the velocity field characterizing the geometrical modification flow.

When ω is a scalar field, the classical material derivative can be applied [45]. However, taking the Lie derivative of a vector field is more delicate as different objects that have three components in an Euclidian space can behave differently under transformation like (1).

For a circulation density like $\boldsymbol{M}$, the Lie derivative reads

$$L_{\mathbf{v}} \boldsymbol{M} = (\nabla \mathbf{v}) \boldsymbol{M}, \tag{17}$$

whereas that of a flux density like $\boldsymbol{J}$ reads

$$L_{\mathbf{v}} \boldsymbol{J} = \boldsymbol{J} \, \mathrm{div}\, \mathbf{v} - (\nabla \mathbf{v})^{\mathbf{T}} \boldsymbol{J}. \tag{18}$$

Furthermore, a material law like $\boldsymbol{H}(\boldsymbol{B}) = \nu\,\mathbf{curl}\,\boldsymbol{A}$ converts a field quantity, $\boldsymbol{B} = \mathbf{curl}\,\boldsymbol{A}$, into another field quantity, $\boldsymbol{H}$, and contains therefore a geometrical conversion operator, called Hodge operator, that depends on the metric. The latter has a non-vanishing Lie derivative when the system deforms. Taking into account the implicit Hodge operator when evaluating the Lie derivative of a material law gives,

$$L_{\mathbf{v}}\boldsymbol{H}(\boldsymbol{B}^\star) = \nu^\partial\,\mathbf{curl}\,L_{\mathbf{v}}\boldsymbol{A}^\star + \nu^\partial\Big((\nabla\mathbf{v})^{\mathbf{T}}\boldsymbol{B}^\star - \boldsymbol{B}^\star\,\mathrm{div}\,\mathbf{v}\Big) + (\nabla\mathbf{v})\,\boldsymbol{H}(\boldsymbol{B}^\star). \tag{19}$$

Using this Lie derivative, we can differentiate under the integral sign of the f,

$$\begin{aligned}\frac{\mathrm{d}f}{\mathrm{d}\tau}(\tau,\rho,\boldsymbol{A}^\star) &= \int_{\Omega(\tau)} L_{\mathbf{v}}F(\tau,\rho,\boldsymbol{A}^\star)\;\mathrm{d}\Omega \\ &= \int_{\Omega(\tau)} \Big(D_\tau F(\tau,\rho,\boldsymbol{A}^\star) + \big\{\mathrm{D}_{\boldsymbol{A}}F(\tau,\rho,\boldsymbol{A}^\star)\big\}\big(L_{\mathbf{v}}\boldsymbol{A}^\star\big)\Big)\;\mathrm{d}\Omega,\end{aligned} \tag{20}$$

where the sensitivity is expressed in terms of the Lie derivative $L_{\mathbf{v}}\boldsymbol{A}^\star$, which represents the evolution of the solution $\boldsymbol{A}^\star$ of the physical problem (2) as the shape parameter τ is changing. The first term in (20) is the partial derivative of the functional,

$$D_\tau F(\tau,\rho,\boldsymbol{A}^\star) = L_{\mathbf{v}}F(\tau,\rho,\boldsymbol{A}^\star)\Big|_{L_{\mathbf{v}}\boldsymbol{A}=0}, \tag{21}$$

whereas the second term is its Fréchet derivative with respect to its field argument, as defined in (8).

Using the adjoint approach, the differentiation of the augmented function (9) with respect to τ yields

$$\begin{aligned}\frac{\mathrm{d}f_a}{\mathrm{d}\tau} = \int_{\Omega(\tau)} \Big(&D_\tau F(\tau,\rho,\boldsymbol{A}^\star) + \big\{\mathrm{D}_{\boldsymbol{A}}F(\tau,\rho,\boldsymbol{A}^\star)\big\}\big(L_{\mathbf{v}}\boldsymbol{A}^\star\big) \\ &- L_{\mathbf{v}}(\nu\,\mathbf{curl}\,\boldsymbol{A}^\star)\cdot\mathbf{curl}\,\boldsymbol{\lambda} + L_{\mathbf{v}}\boldsymbol{J}\cdot\boldsymbol{\lambda} + L_{\mathbf{v}}\boldsymbol{M}\cdot\mathbf{curl}\,\boldsymbol{\lambda}\Big)\,\mathrm{d}\Omega = 0,\end{aligned} \tag{22}$$

where we have already omitted the null term.

Substituting (17), (18) and (19) into (22) yields the linear adjoint system to solve for $L_{\mathbf{v}}\boldsymbol{A}^\star$,

$$\int_{\Omega(\tau)} \Big(\big\{\mathrm{D}_{\boldsymbol{A}}F(\tau,\rho,\boldsymbol{A}^\star)\big\}\big(L_{\mathbf{v}}\boldsymbol{A}^\star\big) - \nu^\partial\,\mathbf{curl}\,\boldsymbol{\lambda}\cdot\mathbf{curl}\,L_{\mathbf{v}}\boldsymbol{A}^\star\Big)\;\mathrm{d}\Omega = 0, \tag{23}$$

which, once discretized, is the same linear system as (13).

The sensitivity with respect to τ is then given by

$$\begin{aligned}\frac{\mathrm{d}f_a}{\mathrm{d}\tau}(\tau,\rho,\boldsymbol{A}^\star,\boldsymbol{\lambda}^\star) = \int_{\Omega(\tau)} \Big(&D_\tau F(\tau,\rho,\boldsymbol{A}^\star) - \nu^\partial\Big((\nabla\mathbf{v})^{\mathbf{T}}\,\mathbf{curl}\,\boldsymbol{A}^\star - \mathbf{curl}\,\boldsymbol{A}^\star\,\mathrm{div}\,\mathbf{v}\Big)\cdot\mathbf{curl}\,\boldsymbol{\lambda}^\star \\ &- (\nabla\mathbf{v})\,\nu\,\mathbf{curl}\,\boldsymbol{A}^\star\cdot\mathbf{curl}\,\boldsymbol{\lambda}^\star + (\boldsymbol{J}\,\mathrm{div}\,\mathbf{v} - (\nabla\mathbf{v})^{\mathbf{T}}\boldsymbol{J})\cdot\boldsymbol{\lambda}^\star + (\nabla\mathbf{v})\boldsymbol{M}\cdot\mathbf{curl}\,\boldsymbol{\lambda}^\star\Big)\;\mathrm{d}\boldsymbol{\Omega}\end{aligned} \tag{24}$$

The obtained sensitivity has a rather large number of terms, which can however either be reused from the finite element solution or evaluated on a support limited to a one layer thick layer of finite elements on both sides of the surfaces involved in the shape variation.

5. Application to the design of a PMSM

Interior permanent magnets synchronous machines (PMSM) suffer from a high level of torque ripple which should be reduced as much as possible, while keeping the average torque above or equal to the nominal torque of the machine. Let us perform a combined shape and topology optimization to determine simultaneously (1) the distance of the PMs from the air gap, the angle between the PMs, both set as shape design variables, noted τ, and also (2) the steel density distribution, noted ρ, defined in the rest of the rotor. We want to smoothen torque with respect to the movement of the rotor, minimizing hence the torque ripple, while preserving an average torque to match the nominal torque of the machine. The combined shape and topology optimization problem (4) reads,

$$\begin{aligned} \min_{\tau,\rho} \quad & f_0(\tau,\rho,\boldsymbol{A}^\star) \equiv \sum_{R=1}^{N_p} \left(T_R - T_{nom}\right)^2 \\ s.t. \quad & f_1(\tau,\rho,\boldsymbol{A}^\star) \equiv \frac{1}{N_p}\sum_{R=1}^{N_p} T_R - T_{nom} \leq 0, \\ & \tau^{min} \leq \tau \leq \tau^{max} \\ & \rho^{min} \leq \rho \leq \rho^{max} \\ & r(\tau,\rho,\boldsymbol{A}^\star,\bar{\boldsymbol{A}}) = 0,\ \forall \bar{\boldsymbol{A}} \end{aligned} \tag{25}$$

A method based on Maxwell's stress tensor is used for the computation of torque. Choosing a circular shell of axial length L_a and surface S_a in the moving band, noted Ω_{mb}, of the airgap of the machine as a closed integration surface that surrounds the rotor, the torque at a given rotor position θ_R reads,

$$T_R = \int_{\Omega_{mb}} \nu_0\ t_g\ B_r\ B_\theta\ \mathrm{d}\Omega, \tag{26}$$

with

$$t_g = 2\pi \frac{L_a}{S_a} \boldsymbol{r}\cdot\boldsymbol{r} \tag{27}$$

being a geometrical coefficient where $\boldsymbol{r}$ is radial vector, $B_r = \boldsymbol{B}^\star \cdot \boldsymbol{e}_r$ and $B_\theta = \boldsymbol{B}^\star \cdot \boldsymbol{e}_\theta$ are the scalar product of $\boldsymbol{B}^\star$ with respectively the radial basis vector $\boldsymbol{e}_r$ and tangential basis vector $\boldsymbol{e}_\theta$.

The design space is limited by physical side constraints either for the shape design variables, $\tau^{min} \leq \tau \leq \tau^{max}$, or the density design variables, $\rho^{min} \leq \rho \leq \rho^{max}$, which are independent from the shape design variables, but involved in the same performance functions.

The evaluation of the performance functions f_0 and f_j, $j = 1, 2$ for a given geometric configuration, τ, and a given material distribution, ρ, requires the knowledge of $\boldsymbol{A}^\star$ for that particular value of τ and ρ, which implies solving anew the nonlinear physical problem (2) at N_p rotor positions and evaluate the torque T_R at each position θ_R, by making use of (26). The repetition of these evaluations is time-consuming for large scale applications.

A sequential convex programming algorithm, MMA [40], is used, coupled with a finite element analysis code [41, 42] and makes use of the sensitivity formulas (14) and (24) derived so far. The results of the optimization problem are summarized in Fig. 3. The entire analysis domain and design domain are discretized using 37,521 nodes and 64,640 triangular elements. The densities are used to interpolate the magnetic reluctivity through a classical SIMP (3) with a penalization parameter p fixed to 3. The optimization process results, after roughly 250 iterations, in PMs with a slightly increased angular openings compared to the original design, indicating that the topology optimization allows, in this particular case, major improvements of

the electrical rotating machine. The torque ripple is reduced by 97% while the average torque is set to the nominal torque of the machine.

A post-processing stage is needed to obtain a manufacturable design, see for instance [46] or more recently [47]. Computer vision technologies to represent the boundary of the void-solid finite element topology optimization result have first been performed in [48]. A density contour approach has also been used in [49], or [50] as well as a geometric reconstruction approach, see for instance [51].

Here we performed a spline-based interpolation of the density isovalues. This then leads to a CAD model which is used for latter design stages as well as e.g. for additive manufacturing purposes, see Fig. 4. However, a drawback inherent to such procedures, is that post-processed results are no longer optimal and may also not comply with the given design criteria, thus slightly deteriorating the topology optimization solutions. In this particular case, the torque ripple is increased by 10% from the one computed with the density field.

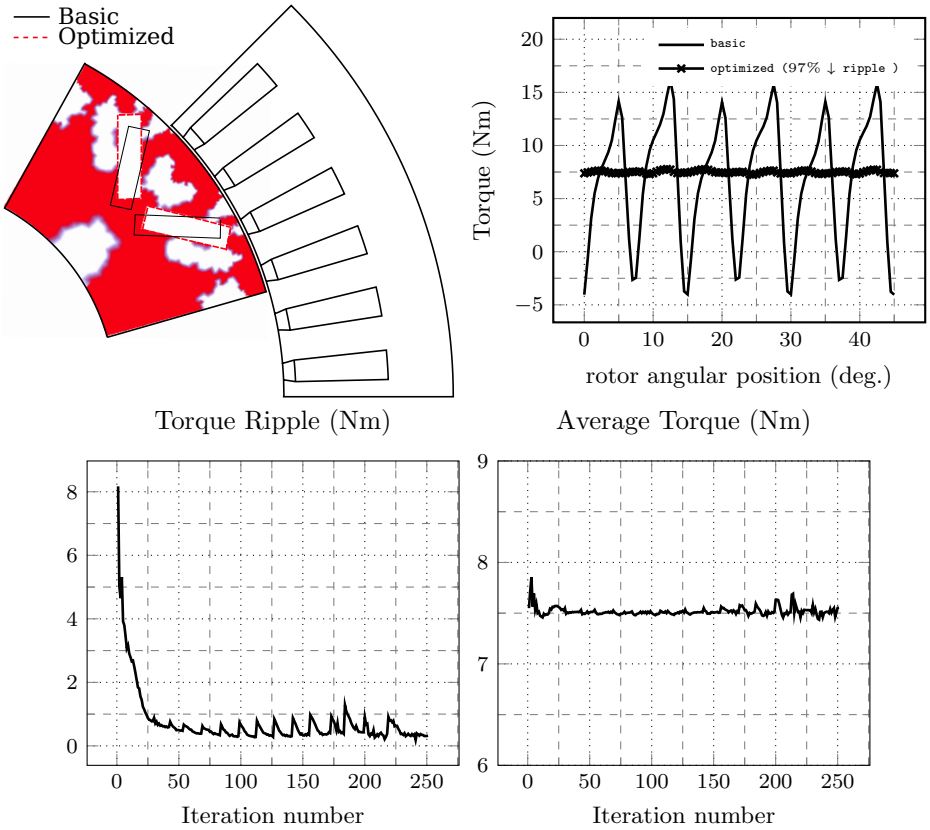

Figure 3: A range of $N_p = 16$ rotor angular positions which covers an angular torque period, from 0 to 16 degrees has been considered and the geometrical configuration of the PMs as well as the steel density distribution in the rotor have been determined simultaneously with a combined shape and topology optimization.

6. Conclusion and perspectives

We have developed a unified tool for handling simultaneously the complex interactions between the material density distribution model of topology optimization and the geometrical

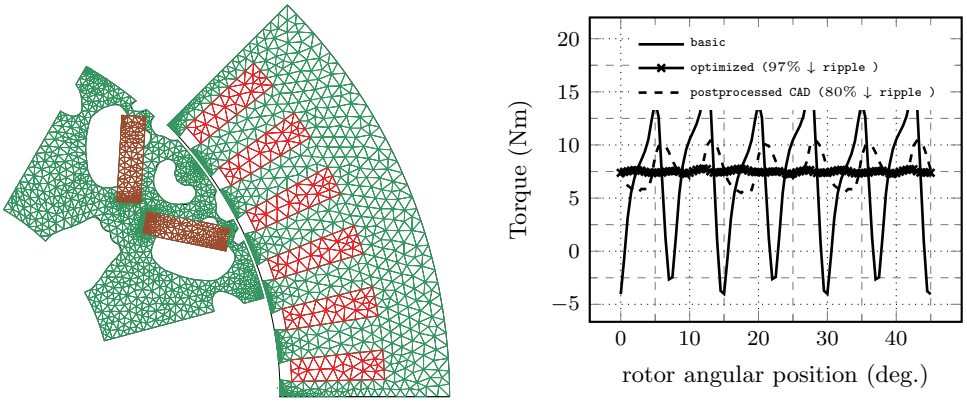

Figure 4: A smooth CAD model of the optimized rotor is obtained manually from the finite element representation of Fig. 3 by making use of spline curves. The geometrical model can hence be used in later design stages.

modifications which occur throughout a shape optimization. Following the general framework of sensitivity analysis derived so far, shape sensitivity is computed efficiently. We can obtain simultaneously the sensitivity with respect to shape and density design variables. The theoretical results gathered in the article have been successfully applied to electro-mechanical optimization of the shape and topology of energy conversion systems which are of a great importance in industry. The design of an electrical synchronous rotating machine with interior permanent magnets, modeled by means of a two-dimensional CAD model coupled to a nonlinear magnetostatic formulation, and aiming to minimize the torque ripple has been successfully obtained in our framework.

Acknowledgments

This work was supported in part by the Walloon Region of Belgium under grant RW-1217703 (WBGreen FEDO) and the Belgian Science Policy under grant IAP P7/02.

References

[1] V. Braibant, C. Fleury, Shape optimal design using b-splines, Computer Methods in Applied Mechanics and Engineering 44 (3) (1984) 247–267.

[2] N. Olhoff, M. P. Bendsøe, J. Rasmussen, On cad-integrated structural topology and design optimization, Computer Methods in Applied Mechanics and Engineering 89 (1-3) (1991) 259–279.

[3] G. Rozvany, Aims, scope, methods, history and unified terminology of computer-aided topology optimization in structural mechanics, Structural and Multidisciplinary optimization 21 (2) (2001) 90–108.

[4] H. A. Eschenauer, N. Olhoff, Topology optimization of continuum structures: a review, Applied Mechanics Reviews 54 (4) (2001) 331–390.

[5] O. Sigmund, K. Maute, Topology optimization approaches, Structural and Multidisciplinary Optimization 48 (6) (2013) 1031–1055.

[6] K.-U. Bletzinger, K. Maute, Towards generalized shape and topology optimization, Engineering Optimization 29 (1-4) (1997) 201–216.

[7] A. N. Christiansen, M. Nobel-Jørgensen, N. Aage, O. Sigmund, J. A. Bærentzen, Topology optimization using an explicit interface representation, Structural and Multidisciplinary Optimization 49 (3) (2014) 387–399.

[8] H. Lian, A. N. Christiansen, D. A. Tortorelli, O. Sigmund, N. Aage, Combined shape and topology optimization for minimization of maximal von mises stress, Structural and Multidisciplinary Optimization 55 (5) (2017) 1541–1557.

[9] M. K. Misztal, K. Erleben, A. Bargteil, J. Fursund, B. B. Christensen, J. A. Bærentzen, R. Bridson, Multiphase flow of immiscible fluids on unstructured moving meshes, IEEE transactions on visualization and computer graphics 20 (1) (2014) 4–16.

[10] S. Osher, J. A. Sethian, Fronts propagating with curvature-dependent speed: algorithms based on hamilton-jacobi formulations, Journal of computational physics 79 (1) (1988) 12–49.

[11] G. Allaire, F. Jouve, A.-M. Toader, A level-set method for shape optimization, Comptes Rendus Mathematique 334 (12) (2002) 1125–1130.

[12] M. Y. Wang, X. Wang, D. Guo, A level set method for structural topology optimization, Computer methods in applied mechanics and engineering 192 (1) (2003) 227–246.

[13] J. Kwack, S. Min, J.-P. Hong, Optimal stator design of interior permanent magnet motor to reduce torque ripple using the level set method, IEEE Transactions on Magnetics 46 (6) (2010) 2108–2111.

[14] M. Hintermüller, A. Laurain, Electrical impedance tomography: from topology to shape., Control & Cybernetics 37 (4).

[15] A. A. Novotny, R. A. Feijóo, E. Taroco, C. Padra, Topological sensitivity analysis, Computer methods in applied mechanics and engineering 192 (7) (2003) 803–829.

[16] B. Hassani, S. M. Tavakkoli, H. Ghasemnejad, Simultaneous shape and topology optimization of shell structures, Structural and Multidisciplinary Optimization 48 (1) (2013) 221–233.

[17] P. Gangl, U. Langer, A. Laurain, H. Meftahi, K. Sturm, Shape optimization of an electric motor subject to nonlinear magnetostatics, SIAM Journal on Scientific Computing 37 (6) (2015) B1002–B1025.

[18] H. Emmendoerfer Jr, E. A. Fancello, Topology optimization with local stress constraint based on level set evolution via reaction–diffusion, Computer Methods in Applied Mechanics and Engineering 305 (2016) 62–88.

[19] K. Yaji, M. Otomori, T. Yamada, K. Izui, S. Nishiwaki, O. Pironneau, Shape and topology optimization based on the convected level set method, Structural and Multidisciplinary Optimization 54 (3) (2016) 659–672.

[20] J. Sokolowski, A. Zochowski, Optimality conditions for simultaneous topology and shape optimization, SIAM journal on control and optimization 42 (4) (2003) 1198–1221.

[21] H. A. Kalameh, O. Pierard, C. Friebel, E. Béchet, Semi-implicit representation of sharp features with level sets, Finite Elements in Analysis and Design 117 (2016) 31–45.

[22] F. Duboeuf, E. Béchet, Embedded solids of any dimension in the x-fem, Finite Elements in Analysis and Design 130 (2017) 80–101.

[23] J. Zhu, W. Zhang, P. Beckers, Integrated layout design of multi-component system, International journal for numerical methods in engineering 78 (6) (2009) 631–651.

[24] J. Zhang, W. Zhang, J. Zhu, L. Xia, Integrated layout design of multi-component systems using xfem and analytical sensitivity analysis, Computer Methods in Applied Mechanics and Engineering 245 (2012) 75–89.

[25] Z. Qian, G. Ananthasuresh, Optimal embedding of rigid objects in the topology design of structures, Mechanics Based Design of Structures and Machines 32 (2) (2004) 165–193.

[26] W. Zhang, L. Xia, J. Zhu, Q. Zhang, Some recent advances in the integrated layout design of multicomponent systems, Journal of Mechanical Design 133 (10) (2011) 104503.

[27] N. H. K. Kyung K. Choi, Structural Sensitivity Analysis and Optimization 1, Springer Science & Business Media, Inc., 2005.

[28] J. Sokolowski, J.-P. Zolesio, Introduction to shape optimization, in: Introduction to Shape Optimization, Springer, 1992, pp. 5–12.

[29] I.-H. Park, J.-L. Coulomb, S.-Y. Hahn, Implementation of continuum sensitivity analysis with existing finite element code, Magnetics, IEEE Transactions on 29 (2) (1993) 1787–1790.

[30] J. Biedinger, D. Lemoine, Shape sensitivity analysis of magnetic forces, Magnetics, IEEE Transactions on 33 (3) (1997) 2309–2316.

[31] R. Hermann, et al., Harley flanders, differential forms with applications to the physical sciences, Bulletin of the American Mathematical Society 70 (4) (1964) 483–487.

[32] F. Henrotte, Handbook for the computation of electromagnetic forces in a continuous medium, Int. Compumag Society Newsletter 24 (2) (2004) 3–9.

[33] R. Hiptmair, J. Li, Shape derivatives in differential forms i: An intrinsic perspective, Annali di Matematica Pura ed Applicata 192 (6) (2013) 1077–1098.

[34] R. Hiptmair, J. Li, Shape derivatives in differential forms ii: Shape derivatives for scattering problems, SAM Seminar for Applied Mathematics, ETH, Zürich, Switzerland, Research Report, 2017.

[35] E. Kuci, F. Henrotte, P. Duysinx, C. Geuzaine, Design sensitivity analysis for shape optimization based on the Lie derivative, Computer Methods in Applied Mechanics and Engineering 317 (2017) 702 – 722.

[36] C. Fleury, L. A. Schmit Jr, Dual methods and approximation concepts in structural synthesis, NASA (1980) CR–3226.

[37] K. Svanberg, The method of moving asymptotes- a new method for structural optimization, International journal for numerical methods in engineering 24 (2) (1987) 359–373.

[38] N. Sadowski, Y. Lefevre, M. Lajoie-Mazenc, J. Cros, Finite element torque calculation in electrical machines while considering the movement, Magnetics, IEEE Transactions on 28 (2) (1992) 1410–1413. doi:10.1109/20.123957.

[39] A. Bossavit, Computational electromagnetism: variational formulations, complementarity, edge elements, Academic Press, 1998.

[40] K. Svanberg, A class of globally convergent optimization methods based on conservative convex separable approximations, SIAM Journal on Optimization (2002) 555–573.

[41] C. Geuzaine, J.-F. Remacle, Gmsh: A 3-D finite element mesh generator with built-in pre- and post-processing facilities, International Journal for Numerical Methods in Engineering 79 (11) (2009) 1309–1331.

[42] P. Dular, C. Geuzaine, A. Genon, W. Legros, An evolutive software environment for teaching finite element methods in electromagnetism, IEEE Transactions on Magnetics 35 (3) (1999) 1682–1685.

[43] M. P. Bendsøe, N. Kikuchi, Generating optimal topologies in structural design using a homogenization method, Computer methods in applied mechanics and engineering 71 (2) (1988) 197–224.

[44] W.-H. Zhang, P. Beckers, C. Fleury, A unified parametric design approach to structural shape optimization, International Journal for Numerical Methods in Engineering 38 (13) (1995) 2283–2292.

[45] J. S. Arora, E. J. Haug, Methods of design sensitivity analysis in structural optimization, AIAA journal 17 (9) (1979) 970–974.

[46] M.-H. Hsu, Y.-L. Hsu, Interpreting three-dimensional structural topology optimization results, Computers & structures 83 (4-5) (2005) 327–337.

[47] T. Zegard, G. H. Paulino, Bridging topology optimization and additive manufacturing, Structural and Multidisciplinary Optimization 53 (1) (2016) 175–192.

[48] M. P. Bendsøe, H. C. Rodrigues, Integrated topology and boundary shape optimization of 2-d solids, Computer Methods in Applied Mechanics and Engineering 87 (1) (1991) 15–34.

[49] A. Kumar, D. Gossard, Synthesis of optimal shape and topology of structures, Journal of Mechanical Design 118 (1) (1996) 68–74.

[50] Y.-L. Hsu, M.-S. Hsu, C.-T. Chen, Interpreting results from topology optimization using density contours, Computers & Structures 79 (10) (2001) 1049–1058.

[51] P.-S. Tang, K.-H. Chang, Integration of topology and shape optimization for design of structural components, Structural and Multidisciplinary Optimization 22 (1) (2001) 65–82.